

# Surface Plasmon Polariton Assisted Organic Solar Cells

Changsoon Kim\*, Jung-Yong Lee\*\*, Peter Peumans\*\*, and Jungsang Kim\*

\* Department of Electrical and Computer Engineering, Duke University  
Durham, North Carolina 27708

\*\* Department of Electrical Engineering, Stanford University  
Stanford, California 94305

## ABSTRACT

We propose a lateral tandem cell system consisting of organic thin-film photovoltaic devices. The crucial element of the system is a surface plasmon polariton (SPP) assisted organic solar cell employing a metallic grating electrode. In the SPP-assisted solar cell, the incident light resonantly excites an SPP mode to increase the optical field intensity in the absorption layer. As a result, a high absorption efficiency is maintained when the thickness of the absorption layer is decreased below the exciton diffusion length, thereby overcoming the ‘exciton diffusion bottleneck’ present in conventional organic solar cells. For a model structure, where an organic multilayer is sandwiched by a planar cathode and a grating anode, both consisting of Ag, we show, using the finite element method, that the absorption efficiency of a 10-nm-thick absorption layer with the absorption coefficient of  $10^5 \text{ cm}^{-1}$  exceeds 80% for TM-polarized incident light with a wavelength of 765 nm. We show that the resonance can be tuned by varying the grating period. We also discuss design guidelines for the lateral tandem cell system, and estimate its performance.

**Keywords:** organic solar cell, surface plasmon, grating

## 1 INTRODUCTION

Unlike conventional inorganic solar cells, absorption of a photon in an organic solar cell creates a tightly bound exciton, which must be dissociated into an electron and a hole to generate electrical power [1], [2]. Since the efficient dissociation of the excitons occurs at a donor-acceptor (DA) interface, ‘useful’ excitons that eventually contribute to electrical power are those generated within a diffusion length from the DA interface. The diffusion length ( $L_D < \sim 10 \text{ nm}$ ) of excitons in organic semiconductors, both in polymeric and small molecular materials, is in general smaller than the optical absorption length ( $1/\alpha \sim 100 \text{ nm}$ , where  $\alpha$  is the absorption coefficient), presenting an inherent trade-off between the efficiencies of exciton dissociation and photon absorption (so-called ‘exciton diffusion bottleneck’) [3]. Optical resonances can be utilized to enhance the light absorption without increasing the thickness of the ac-

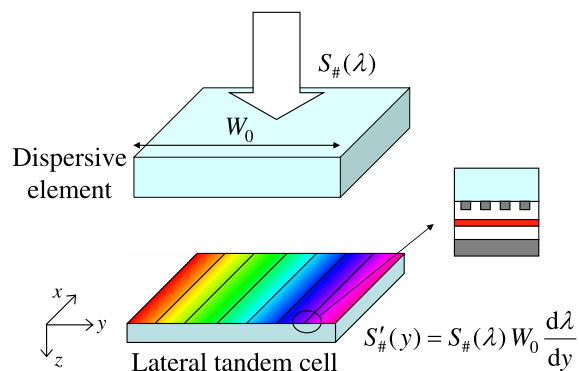


Figure 1: Schematic configuration of a lateral tandem cell system.

tive layer beyond  $L_D$ . However, there exists an inherent trade-off between the magnitude of the enhancement and the bandwidth over which it occurs. Here, we propose a lateral tandem cell (LTC) system capable of overcoming this trade-off. The LTC consists of many sub-cells that are connected in series. The resonance we exploit is that of a surface plasmon polariton (SPP) mode present in an organic solar cell employing a metallic grating electrode, and the tunability of the resonance is demonstrated by numerical calculations based on the finite-element method. The LTC system offers a straightforward platform for both optical and electrical optimization. We discuss design guidelines for the LTC system, and estimate its performance.

## 2 LATERAL TANDEM CELL - CONCEPT

Figure 1 shows a basic concept of a lateral tandem cell (LTC). The dispersive element spatially separates the incoming solar photons according to their wavelengths ( $\lambda$ ) to achieve a mapping between  $\lambda$  and the position ( $y$ ) on the LTC, and the local photonic and electronic properties of the LTC are optimally tuned at all  $y$ . Specifically, the structure of the device is continuously varied along the  $y$ -direction to enable the optical fields incident on  $y$  to resonantly excite the cell at that location. Furthermore, organic materials are chosen so that (1) the absorption spectrum of the optically active

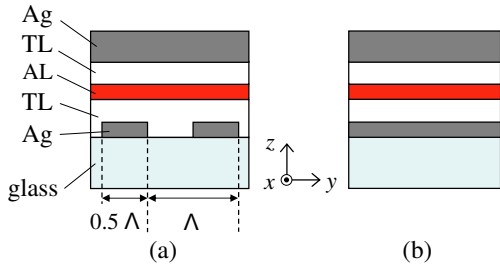


Figure 2: (a) Layer structure of a model device. TL: charge transport layer, AL: absorption layer,  $\Lambda$ : grating period. (b) Layer structure of a planar device, where the grating electrode in (a) is replaced by a planar layer.

material matches well with  $\lambda(y)$  and (2) energy loss associated with exciton dissociation and charge transport processes is minimized to obtain a large open-circuit voltage ( $V_{OC}$ ) and fill factor ( $FF$ ). The LTC is divided into sub-cells, which are connected in series with the adjacent sub-cells. The short-circuit current that each sub-cell generates can be tuned by varying the width (along the  $y$ -axis) of the cell, providing a straightforward method for balancing the short-circuit currents, as required for a tandem cell connected in series [4].

### 3 SURFACE PLASMON POLARITON ASSISTED ORGANIC SOLAR CELLS

A model device that we consider is schematically shown in Fig. 2(a). It has a structure comprising: glass substrate / 20-nm-thick Ag grating electrode / 45-nm-thick charge transport layer / 10-nm-thick absorption layer / 25-nm-thick charge transport layer / 150-nm-thick Ag electrode. The charge transport layers have a refractive index of  $\tilde{n} = 2$ . The absorption layer has a refractive index of  $\tilde{n} = 2 + in'$ , with  $n'$  varying with wavelengths to yield  $\alpha = 10^5 \text{ cm}^{-1}$  in all spectral regions. First, we calculate the photonic band structure of a planar device shown in Fig. 2(b), where the grating electrode in the model device is replaced with a planar Ag layer. By considering the grating electrode as perturbation of the planar electrode, we semi-quantitatively understand the dependence of resonant energy on the grating period. The rigorous calculations for the model device are achieved by performing electromagnetic and excitonic analyses using the finite-element method. In this paper, we limited our analysis to the TM-polarization (the magnetic field  $\parallel x$ ).

#### 3.1 Planar structure

Figure 3(a) shows the complex photonic band structure, i.e. energy ( $E$ ) vs. complex in-plane wavevector ( $k$ ), of the planar device. The mode drawn with

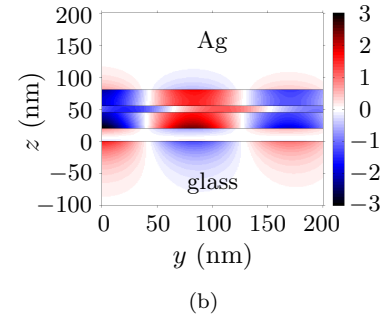
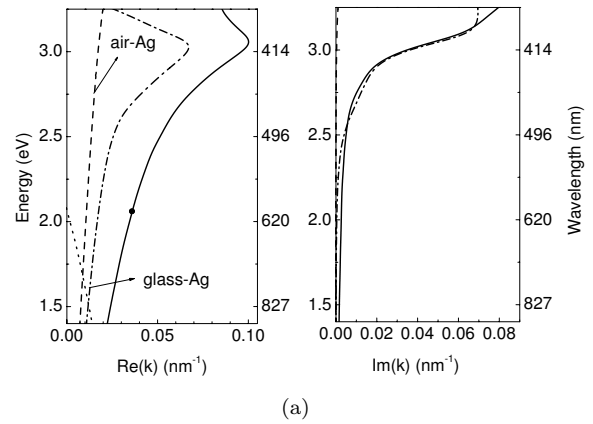


Figure 3: (a) Complex photonic band diagram of the planar device for TM-polarization. Dashed line: surface plasmon polariton (SPP) mode propagating along the air-Ag interface. Dash-dot line: SPP mode along the glass-Ag interface. Solid line: SPP mode that has an appreciable field intensity in the organic layers. Dotted line in the left panel: Solid line folded at  $\Re(k) = 0.018 \text{ nm}^{-1}$ . (b)  $z$ -component of the electric field of the mode at  $(k, E) = (0.036 + i0.0028 \text{ nm}^{-1}, 2.07 \text{ eV})$  indicated with a dot in (a).

a dashed line corresponds to a surface plasmon mode propagating along the air-Ag interface, while the mode drawn with a dash-dot line corresponds to a surface plasmon mode propagating along the glass-Ag interface. The third mode represented as a solid line is our main interest. As shown in Fig. 3(b), it is a surface plasmon polariton (SPP) mode with an appreciable field intensity in the organic layers. The SPP mode lies below the light line corresponding to the glass layer, and hence cannot be excited by external fields. However, the introduction of the grating electrode ‘folds’ the band diagram, allowing the external fields to couple with the SPP mode. For a given grating period ( $\Lambda$ ), the intersection of the folded branch at the  $E$  axis can be considered a zeroth order estimation of the photon energy that resonantly couples with the device. For example, to get a coupling at  $\lambda = 600 \text{ nm}$  ( $E = 2.07 \text{ eV}$ ), the boundary of the 1st Brillouin zone needs to be at  $\pi/\Lambda = 0.018 \text{ nm}^{-1}$ ,

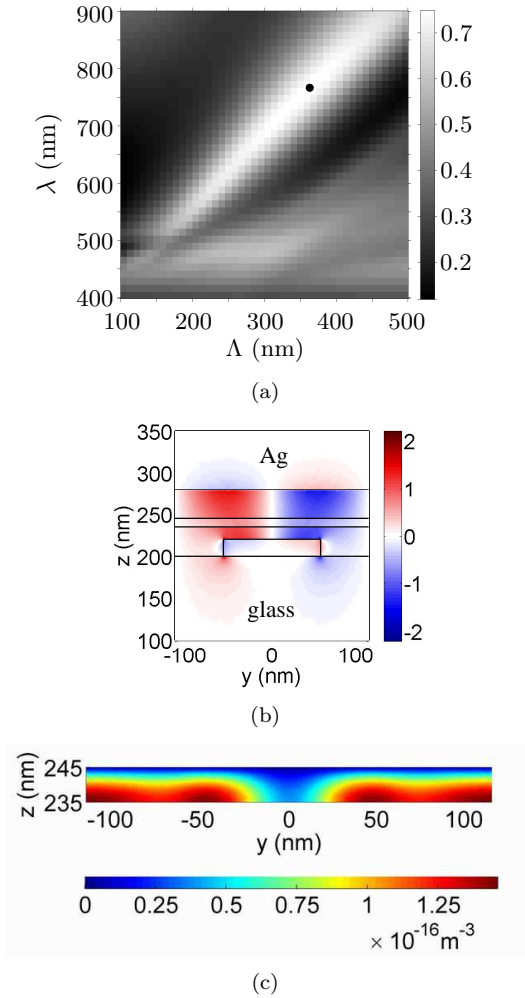


Figure 4: (a) External quantum efficiency ( $\eta_{ext}$ ) of a model device as a function of the grating period ( $\Lambda$ ) and illumination wavelength ( $\lambda$ ). A black dot represents  $(\Lambda, \lambda)$  that maximizes  $\eta_{ext}$ . (b)  $z$ -component of the electric field corresponding to  $(\Lambda, \lambda) = (232 \text{ nm}, 600 \text{ nm})$ . (c) Exciton density profile for  $(\Lambda, \lambda) = (232 \text{ nm}, 600 \text{ nm})$ .

indicating that  $\Lambda = 175 \text{ nm}$ . We expect that the resonance can be tuned by varying the grating period; as  $\Lambda$  increases, the coupling occurs at a lower energy. Furthermore, Fig. 3(a) shows that the SPP mode becomes lossy as  $\lambda < 500 \text{ nm}$ , which is due to the absorption in Ag. Therefore, we expect the absorption efficiency of the organic layer in the model device to decrease as  $\lambda$  decreases below  $500 \text{ nm}$ , limiting the device efficiency.

### 3.2 Grating structure

We calculate the external quantum efficiency ( $\eta_{ext}$ , defined as the probability that an incident photon creates a charge carrier collected at the electrodes) spectrum of the model device as  $\Lambda$  is varied. First, we calculate the absorption of electromagnetic energy in the

absorption layer for the case of normal incidence. Subsequently, steady-state exciton density profile was calculated by solving a diffusion equation under the following assumptions: the diffusion length ( $L_D$ ) of the excitons is  $20 \text{ nm}$ ; the exciton generation rate is proportional to the time-averaged absorbed power; the exciton dissociation velocity at the interface between the absorption and upper charge transport layers is infinite, while that at the interface between the absorption and lower charge transport layers is zero. The short-circuit current is then calculated from the steady-state exciton density profile, from which we obtain  $\eta_{ext}$ . The similar analysis for planar multilayer structures was outlined in detail in [1]. Both electromagnetic and diffusion simulations were done using a finite-element method software package [5].

Figure 4(a) shows the calculated  $\eta_{ext}$  as a function of  $(\Lambda, \lambda)$ . The expected dependency (resonant energy decreases with increasing  $\Lambda$ ) is clearly visible. The absorption efficiency of the  $10\text{-nm}$ -thick absorption layer ( $\eta_{abs}$ , defined as the probability that an incident photon is absorbed in the absorption layer) peaks at  $0.81$  when  $\lambda = 765 \text{ nm}$  ( $\Lambda = 364 \text{ nm}$ ). On this condition,  $\eta_{ext} = 0.75$  as marked by a black dot in Fig. 4(a), indicating that  $92\%$  of the photo-generated excitons ( $L_D = 20 \text{ nm}$ ) reach the interface between the absorption layer and the upper charge transport layer. By varying  $\Lambda$  along the bright white region in Fig. 4(a), we can achieve  $\eta_{abs} > 0.7$  over a large spectral region ranging from  $\lambda = 550 \text{ nm}$  to  $900 \text{ nm}$ .  $\Lambda$  that maximizes  $\eta_{ext}$  for  $\lambda = 600 \text{ nm}$  is  $232 \text{ nm}$ , which is larger than our zeroth order estimation ( $175 \text{ nm}$ ) in the previous section. However, the  $z$ -component of the corresponding electric field shown in Fig. 4(b) resembles that shown in Fig. 3(b), confirming that our perturbative approach is valid.

## 4 LATERAL TANDEM CELL - DESIGN

To demonstrate that an LTC can enhance the device performance compared to conventional devices, we perform an analysis under the following assumptions; a dispersive element in the LTC is capable of achieving a spectral distribution,  $\lambda(y)$ , at the surface of the LTC from the incoming solar photon flux; the LTC consists of  $N_{sc}$  sub-cells that are connected to the adjacent sub-cells in series; in all spectral regions where there is non-negligible amount of photon energy, an absorption material with  $\alpha \simeq 10^5 \text{ cm}^{-1}$  is available. Under solar illumination with a photon number flux per wavelength,  $S_{\#}(\lambda)$ , a region of the LTC ranging from  $y = y_i$  to  $y_j$  generates a short-circuit current per unit length (in the

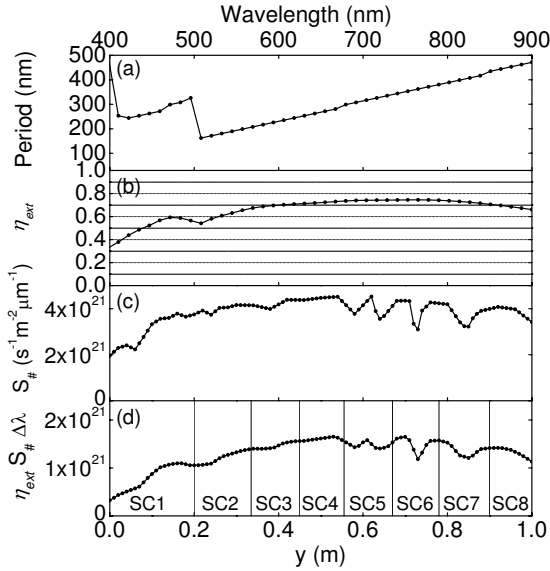


Figure 5: (a) Grating period maximizing the external quantum efficiency at all locations on a lateral tandem cell. We assume that the wavelength of photons incident on  $y$  linearly varies from 400 nm to 900 nm. (b) External quantum efficiency as a function of position. (c) Photon number flux per wavelength with an integrated power of 100 mW/cm<sup>2</sup>. (d) Integrand in Eq. (1).  $\Delta\lambda = 500$  nm. The vertical lines represent the partitioning of the lateral tandem cell into 8 sub-cells. SC*i*:  $i^{\text{th}}$  sub-cell.

$x$ -direction)

$$\begin{aligned}
 I'_{SC} &= e \int_{y_i}^{y_j} \eta_{ext}(y) S'_{\#}(y) dy \\
 &= e \int_{y_i}^{y_j} \eta_{ext}(y) S_{\#}(\lambda) W_0 \frac{d\lambda}{dy} dy, \quad (1)
 \end{aligned}$$

where  $S'_{\#}(y)$  is the photon number flux on the LTC surface at  $y$ ,  $W_0$  is the width of the dispersive element, and  $e$  is the electron charge. For given  $\eta_{ext}(y)$  and  $\lambda(y)$ , evaluation of Eq. (1) over the entire LTC length is a conserved quantity, and is defined to be  $I'_{SC,tot}$ . To maximize the power-conversion efficiency ( $\eta_P$ ), the LTC is partitioned into  $N_{sc}$  sub-cells, each generating the identical short-circuit current,  $I'_{SC,tot}/N_{sc}$ . This partitioning is achieved in a straightforward manner by successively determining the widths of the sub-cells. When  $V_{OC}^{(i)}$  and  $FF^{(i)}$  denote, respectively, the open-circuit voltage and the fill factor of the  $i^{\text{th}}$  sub-cell,  $\eta_P$  of the LTC is given by

$$\eta_P = \frac{I'_{SC,tot} \left\{ \frac{1}{N_{sc}} \sum_i V_{OC}^{(i)} FF^{(i)} \right\}}{W_0 \int S_{\#}(\lambda) \frac{hc}{\lambda} d\lambda}, \quad (2)$$

where  $h$  is Planck's constant, and  $c$  is the speed of light in vacuum. The advantage of the LTC approach is apparent in Eq. (2). Since the local photonic property of

the sub-cells is optimized to allow a very thin ( $\sim L_D$ ) active material to efficiently absorb the incident photons, the LTC maximizes  $I'_{SC,tot}$ . Furthermore, the energetics and charge transport property of the organic materials in each sub-cell are optimized to increase the terms in the curly brackets.

We estimate  $\eta_P$  for an LTC where the sub-cells are the SPP-assisted cells described in the previous section. First, from the result shown in Fig. 4(a), we calculate the grating period at each location along the  $y$ -direction [ $\Lambda_{max}(y)$ ] that maximizes  $\eta_{ext}$ , assuming that  $\lambda(y)$  increases linearly from 400 nm to 900 nm over the width of the LTC ( $W_{LTC}$ ). We further assume that  $W_{LTC} = W_0$ .  $\Lambda_{max}(y)$  varies almost linearly with  $y$  over a large spectral region ( $\lambda$  from 500 nm to 900 nm). By continuously varying  $\Lambda$  along the  $y$ -direction, we can achieve  $\eta_{ext} > 0.7$  for  $\lambda = 595$  nm to 860 nm.  $I'_{SC,tot}$  under *TM*-polarized AM1.5 solar illumination with an integrated intensity of 100 mW/cm<sup>2</sup> is proportional to the area under the curve shown in Fig. 5 (d), and is found to be 210 A/m. Figure 5 (d) also shows the width of each sub-cell with the identical short-circuit current. Assuming that  $V_{OC}^{(i)} = (hc) / (e \lambda(y^{(i)})) - 0.8$  V, and  $FF^{(i)} = 0.7$ , where  $y^{(i)}$  is the location of the right boundary of the  $i^{\text{th}}$  sub-cell,  $\eta_{P,TM} = 15\%$ . Since we consider the *TM*-polarized illumination only, the lower bound of  $\eta_P$  for the unpolarized case is 7.5%. However, we note that  $\eta_P$  can be substantially increased if the device structure is optimized for both polarizations.

## 5 CONCLUSION

We proposed an LTC system consisting of SPP-assisted organic solar cells. Our analysis based on the finite-element method showed that a SPP resonance present in such devices enables a 10-nm-thick absorption layer to absorb 81% of the incident power at  $\lambda = 765$  nm. The tunability of the resonance makes the SPP-assisted cell a good candidate to be used in a system where photons in the solar spectrum are delivered to their corresponding matched cells. We provided design guidelines for the LTC system, and estimated its performance.

## REFERENCES

- [1] P. Peumans, A. Yakimov, and S. R. Forrest, *J. Appl. Phys.*, **93**, 3693 (2003).
- [2] H. Hoppe and N. S. Sariciftci, *J. Mater. Res.*, **19**, 1924 (2004).
- [3] S. R. Forrest, *MRS Bull.*, **30**, 28 (2005).
- [4] A. Yakimov and S. R. Forrest, *Appl. Phys. Lett.*, **80**, 1667 (2002).
- [5] COMSOL, Inc., Burlington, MA 01803.